8B.2 IMPACT OF INNER CORE TROPICAL CYCLONE STRUCTURE ON THE POTENTIAL FOR RAPID INTENSIFICATION[†]

Jonathan L. Vigh*
NCAR[†] Research Applications Laboratory, Boulder, Colorado

Christopher M. Rozoff
Cooperative Institute for Meteorological Satellite Studies/UW-Madison, Madison, Wisconsin

1. INTRODUCTION

Data from a 22-year sample of Vortex Data Messages (VDMs) reveal that immature tropical cyclones (TCs) possess a wide variety of vortex structures at the time of initial eye formation. Such structures may be categorized into three groups according to the relation between the initial eye radius and the radius of maximum winds (RMW, defined as the time-trended lower bound of the radius of the flight-level maximum wind). In the first group, the immature TC structure closely resembles the canonical structure of more mature TCs, wherein the RMW is of a similar radial scale as the initial eye radius. In the second group, the RMW is more than twice the initial eye radius. In the final, smaller group, the RMW is found to be less than the initial eye radius (a situation that should not happen according to conventional understanding). These results highlight the fact that structure of immature TCs is not well understood. Since the majority of rapid intensification (RI)[1] events commence when TCs are at relatively weak intensities (25-50 kt), further investigation of this class of storms is warranted.

The structures of immature TCs likely have a profound impact on the subsequent intensity and structure changes. A long line of theoretical, observational, and modeling research suggests that a strong intensification response occurs in the tropical cyclone (TC)-scale vortex when diabatic heating occurs in the high inertial stability region of the TC (Shapiro and Willoughby 1982; Schubert and Hack 1982; Willoughby et al. 1984; van Delden 1989; Pendergrass and Willoughby 2009; Vigh and Schubert 2009). In immature TCs, however, the region of high inertial stability develops concurrently during intensification. One might hypothesize that the structure of the wind field in immature TCs functions somewhat like a manifold that controls and modifies the expression of the TC's convective elements back onto the vortex scale. In this view, the evolving shape of the TC's wind field is analogous to DNA, controlling the potential for RI.

Before proceeding, it is helpful ask some questions. What types of immature storm structures are most supportive of intensification? Are parameters such as the scale of the inner core (e.g. the radius of maximum winds) important? Are there any periods during a storm's development when structural markers are particularly effective?

This work seeks to determine which observationally-based structural measures, if any, have predictive value for a storm's future intensity change.

2. DATA AND METHODS

This study uses the VDM-based Structure and Intensity Data Set, as described in Vigh et al. (2012).[2]. Synthesized from the VDMs transmitted by routine aircraft reconnaissance from 1989–2011, this data set contains dozens of parameters from over 5700 VDMs. Observations occur at a relatively high frequency whenever a plane is in a storm (fixes are typically taken every 1.5 to 3 h, with gaps between planes typically of 4 to 12 h in duration). The data set provides intensity parameters such as the flight level maximum wind speed (FL $v_{\max}$) and the minimum central pressure ($p_{\min}$), the radius of maximum winds ($r_{\max}$), and thermodynamic quantities such as the maximum eye temperature at flight level (T_{eye}), the minimum dew point temperature ($T_{\text{d,eye}}$) and associated dew point temperature depression at that location ($T_{\text{DEP,eye}}$). The data set also contains information on

* *Corresponding author address:* Jonathan Vigh, National Center for Atmospheric Research, P.O. Box 3000, Boulder, CO 80307-3000; e-mail: jvigh@ucar.edu

[†] The National Center for Atmospheric Research is sponsored by the National Science Foundation.

[1] Here, rapid intensification (RI) is defined as a 30 kt intensity change over 24 h.

[2] The first author plans to release the VDM structure and intensity data set to the research community later in 2012. Please check the following location for updates: http://www.ral.ucar.edu/staff/jvigh/vdm/. Detailed graphical presentations of the VDM and Best Track data for each storm are available at: http://www.ral.ucar.edu/hurricanes/structure/plots/.

whether an eye was present (as determined by aircraft-based radar), and how large it was (given by the eye radius, r_{eye}).

Next, we set out to determine which structure metrics are useful for predicting future intensity change. To start off, one might imagine that the overall size of the inner core could be an important metric. r_{eye} and r_{max} both offer information about the scale of the inner core. Specifically, the time-trended lower bound r_{max} offers an important clue about the radial location in which the storm's inflow may begin to transition to upward motion in the eye wall, while r_{eye} offers information about the inner radius of the eyewall, and therefore the inner radial limit of diabatic heating.

r_{eye} and r_{max} can also be combined with the intensity parameter to form a variety of dynamically-motivated quantities that measure different aspects of storm structure. Figure 1 shows a schematic of some possible combinations. Examples include: (a) the region of diabatically-important heating that occurs between the eyewall and the r_{max}, computed as $r_{max} - r_{eye}$; (b) the ratio of r_{max} to r_{eye}, which indicates the relative scale of the dynamically-important heating region to the scale of the diabatic heating; (c) the minimum Rossby length found in the storm, $\lambda_{R,min}$, which sets the dynamical length scale of how far the warming response extends in the vortex as a result of diabatic heating; (d) the dynamical eye size, Ξ, which is computed as the ratio of the r_{eye} and $\lambda_{R,min}$; and (e) dynamically-efficient heating area ratio (DEHA) which combines the ideas behind metrics (a) and (d). Note that the $\lambda_{R,min}$ used here is a somewhat crude approximation that neglects variations in the static stability. Also, since the VDMs do not contain information about the full radial gradient of the tangential wind speed, the vorticity expression is approximated by using just the first term ($f + 2v/r$). In order to compute this quantity, the v is taken to be the highest FL v_{max} measured by aircraft for a given fix, while r is taken to be the r_{max} associated with that wind measurement.

3. RESULTS

To examine the utility of structure metrics for intensity prediction, scatter plot analysis was used to measure the strength of relationships between the various observationally-based structural measures and the subsequent 24-h intensity changes. A total of 77 immature TCs are available in the data sample. These cases are comprised of Atlantic TCs that occurred from 1989-2011. The time of eye formation is used as the baseline time point for comparison of the structural metrics. The 24-h intensity change is computed by interpolating the Best Track intensity values (BT v_{max}) to the baseline time, and the time point 24-h after that time. Cases were eliminated if the storm came within 25 km of landfall during the 24-h period after eye formation. This reduces the number of cases from 77 to approximately 60. A single value regression model is built using simple regression. The strength of the relationship is taken to be the variance explained by the model.

Before showing the scatter plots for the various structure metrics, it is helpful to first examine scatter plots for environmental parameters known to have a strong relationship with subsequent intensity change. The first such parameter is the deep layer vertical wind shear of the storm's environment. This quantity is typically taken as the vector difference between the wind at 850 hPa and 200 hPa. Here, the predictor SHDC from the Statistical Hurricane Intensity Prediction Scheme (SHIPS) is used to represent the observed deep layer vertical wind shear. This value is computed from the analyzed wind field of a global model by first removing the vortex, then averaging the deep layer shear (850 hPa – 200 hPa) over an annulus (from $r = 0$ to 500 km) centered on the storm center. A scatter plot of the resulting SHDC values vs. 24-h intensity change is shown in Fig. 2. As expected, the relationship is strong and inverse, with this one parameter alone explaining 35% of the variance of subsequent 24-h intensity change (DV24). The Maximum Potential Intensity (MPI) is another environmental predictor known to have a strong influence on DV24. Fig. 3 shows the relationship between the SHIPS quantity for MPI (VMPI, computed using the Bister and Emanuel 1998 formulation of MPI) vs. DV24. The relationship is strong and positive, explaining nearly 19% of the total variance.

Figure 4 shows a scatter plot of the first structure metric, the time-trended lower bound r_{eye} vs. DV24. The relationship is weak and positive, indicating that storms with larger eye radii tend to intensify more strongly. The relationship is quite weak though, and only explains 4.3% of the variance. Figure 5 shows a similar plot for the lower bound r_{max}. The relationship of this metric is very poor, explaining just 1.5% of the variance. This illustrates that while r_{eye} and r_{max} may tend to be related in an overall sense, their predictive value may be quite differ. In contrast, Fig. 6 shows a scatter plot of the *upper bound* of r_{max} vs. DV24. The relationship is inverse, indicating that storms with large envelopes of wind maxima tend to intensify less than those whose outer maxima are confined to relatively smaller radii. This relationship explains 4.1% of the variance.

The structural/dynamical metrics that attempt to quantify some measure of the dynamically-efficient heating region (e.g. $r_{max} - r_{eye}$, the ratio of r_{max} to r_{eye}, or DEHA) all fared poorly and are not shown here. There are essentially no meaningful relationships between these quantities and DV24. The $\lambda_{R,min}$ displayed a

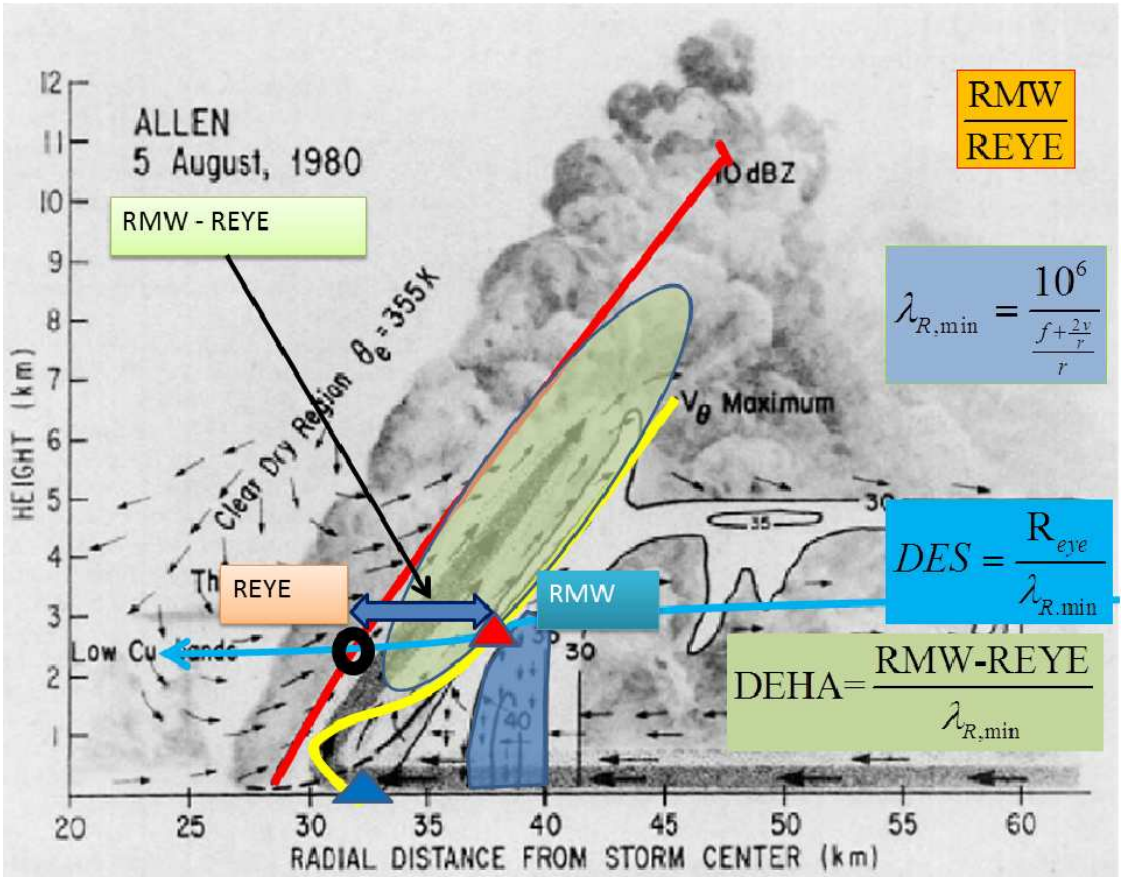

Figure 1: The underlying image of this figure is a schematic cross section (Fig. 19 from Jorgensen 1984) that shows the radial locations of the clouds and precipitation, the sloping radius of maximum wind (RMW), the edge of the eyewall boundary, and the airflow through the eyewall for as determined from composites of radar and kinematic data in Hurricane Allen on 5 August 1980. Various structural aspects are enhanced here, such as the sloping eye radius (as determined by the composite mean 10 dBZ reflectivity contour, shown by a thick red line), the estimated location of maximum tangential wind (thick yellow curve) the region of heaviest rainfall (dark blue shading), and the expected region of dynamically-efficient diabatic heating (found between the sloping edge of the eyewall, and the RMW surface, pale green shading). The observationally-based VDM parameters that correspond to a typical aircraft flight path through the storm (indicated by a blue curve) are superimposed on the schematic. These include the radial location of the maximum flight level wind (FL $r_{\max}$, filled red triangle), the radial location of the surface $r_{\max}$ (filled blue triangle), and the eye radius at flight level (hollow black circle). The various combined structural/dynamical metrics that can be formed from these VDM parameters are annotated on the figure and are described in the text.

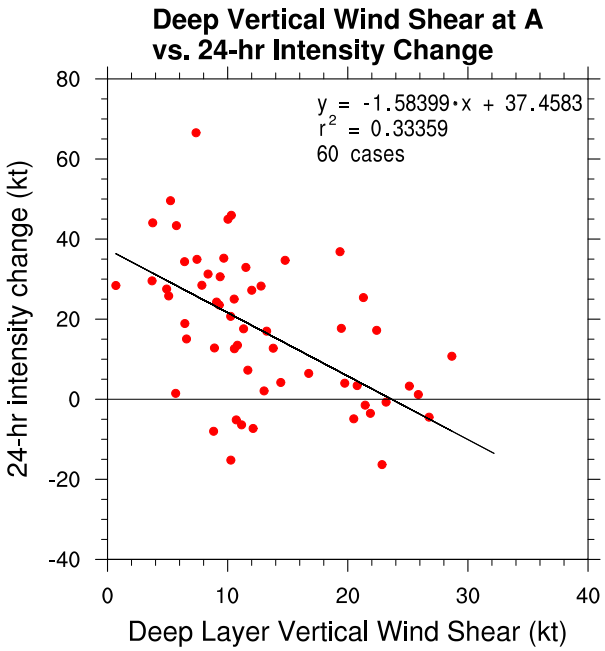

Figure 2: A scatter plot of SHIPS parameter for the deep layer vertical wind shear of the storm environment (SHDC) vs. the subsequent 24-h intensity change after eye formation. The best-fit linear regression line that corresponds to the single variable regression model is also shown.

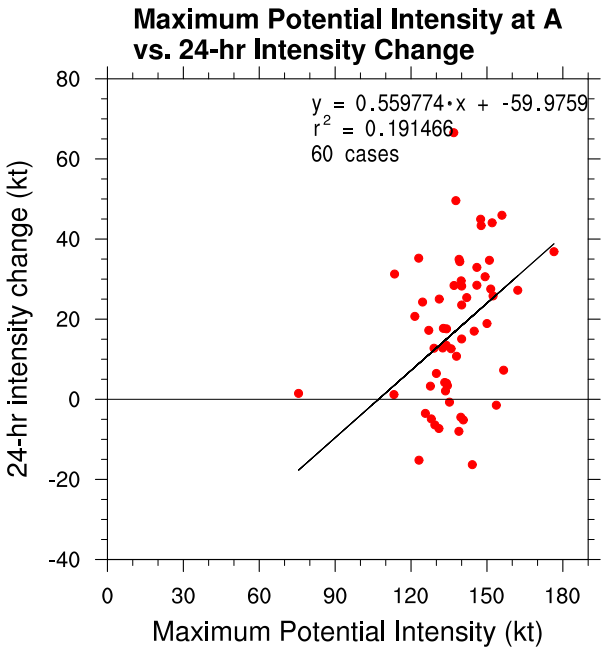

Figure 3: A scatter plot of SHIPS parameter for the Maximum Potential Intensity (VMPI) vs. the subsequent 24-h intensity change after eye formation.

weak, inverse relationship, explaining 1.6% of the variance.

Fig. 7 shows the scatter plot for Ξ vs. DV24. This is by far the strongest relationship of any of the structural/dynamical metrics, explaining 23.7% of the variance. Due to the fact that both r_{eye} and r_{max} may not always be available at the first aircraft fix to observe an eye, this quantity is only available in about three quarters of all the cases (the number of cases is reduced from 60 to 44). To get around this impediment, it is possible to compute the time-trended upper bound Ξ. The scatter plot for this quantity is shown in Fig. 8. With more cases included, this quantify still explains 15.7% of the total variance. The strength of the relationship is on par with that of VMPI.

To determine whether the predictive power of Ξ holds at other times in the storm's life-cycle, even when an eye is not present, a similar metric was crafted by dividing the r_{max} by $\lambda_{\text{R,min}}$. A scatter plot of this new "Dynamical Vortex Scale" (DVS) vs. DV24 is shown in Fig. 9. Compared to Ξ, this new quantity has a comparably strong, positive relationship with future intensity change. It explains 16.3% of the variance.

To test whether DVS has predictive power at earlier or later periods from the point of eye formation, scatter plots were created for DVS vs. the 24-h intensity change following the times when the storm first reached the fixed intensity thresholds of 45, 55, and 65 kt. The variance explained is 2.6%, 1.5%, and 11.8%, respectively. It is intriguing that the relationship seems to grow stronger at higher intensity. Nevertheless, the strongest predictive power seems to be found at the actual time of eye formation rather than a fixed intensity threshold.

Fig. 10 shows the individual intensity curves, as well as composite means, for cases stratified by Ξ at the time when the eye first appears. Storms with large Ξ tend to undergo strong intensification. The composite mean intensity of the large Ξ cases rises strongly, while it barely increases for the storms with a small Ξ. This analysis adds weight to the idea that Ξ has significant predictive value for predicting future intensity change. A similar stratification by the initial r_{max} (not shown) does not show nearly as much influence.

As a final analysis, the number of storms undergoing RI were counted for each grouping of Ξ. Of the small Ξ storms, 4 out of 25 underwent RI (16%). Of the moderate Ξ storms, 3 out of 19 underwent RI (15.7%). Of the large Ξ storms, fully 10 out of 17 underwent RI (58.9%). Supporting summary tables are available at: http://www.ral.ucar.edu/staff/jvigh/vdm/des/.

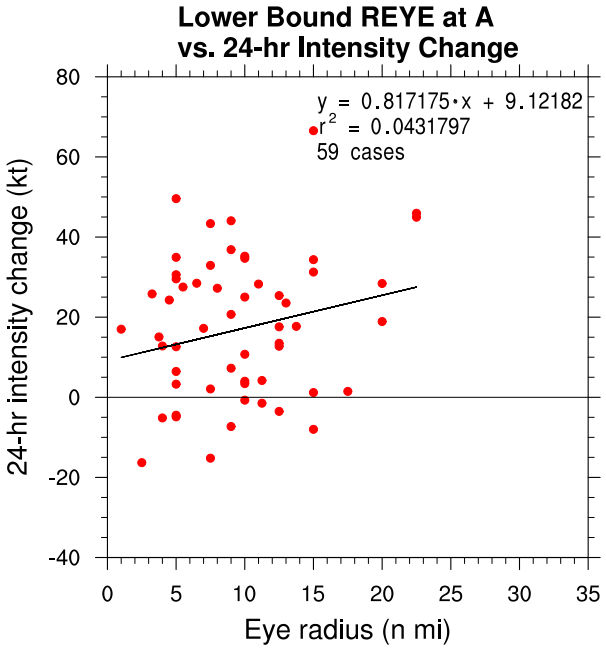

Figure 4: A scatter plot of lower bound r_{eye} vs. the subsequent 24-h intensity change after eye formation.

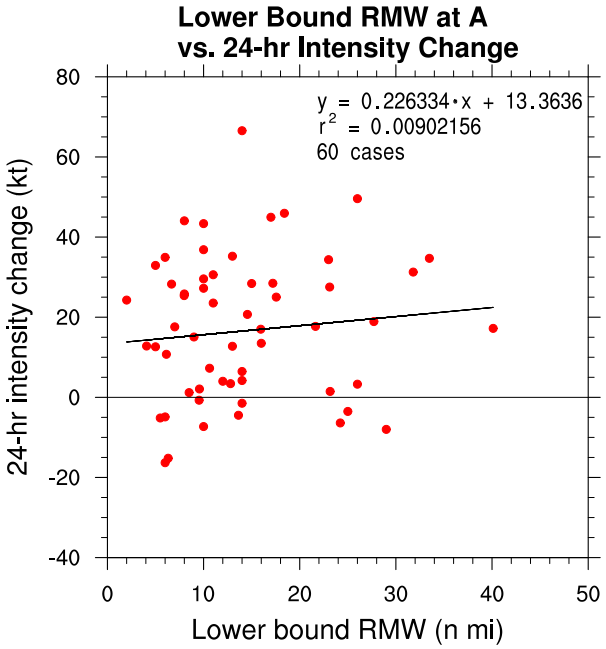

Figure 5: A scatter plot of lower bound r_{max} vs. the subsequent 24-h intensity change after eye formation.

4. CONCLUSIONS

This work has examined the utility of various structure metrics for the prediction of future intensity change for a large sample of immature storms. Most size-based metrics were found to have weak predictive value, although r_{eye} and upper bound r_{max} both explained about 4% of the variance of future intensity change. The dynamical eye size, Ξ, has been found to possess strong predictive value of the 24-h future intensity. **Nearly 60% of storms with initially large dynamical eye size (**> 1.2**) undergo rapidly intensification.** Depending on the method by which it is calculated, Ξ explains as much or more predictive value than the environmental MPI (as determined from the SHIPS predictor VMPI).

How can we understand this finding? Looking in more depth at the scatter plot for Ξ (Fig. 8), it seems that storms with large Ξ preferentially strengthen, often rapidly, while storms with small Ξ can also strengthen rapidly, but also can rapidly weaken. What factor favors RI in storms with large Ξ? We speculate that the storms that form large eyes tend to do so at higher intensities (e.g., 65 kt) than storms that form small eyes (e.g., 50 kt).[3] The higher intensity of the large-eye storms likely counteracts the influence of the larger r_{max} in the computation of the Rossby length. All other things being equal, a larger eye leads to a larger Ξ value. This is reflected by the fact that DVS has greater predictive power at higher fixed intensity thresholds. Thus, large eye storms, forming eyes at higher intensities, may have several advantages. First, the physical scale of the region of dynamically-efficient heating is large compared with the Rossby length, leading to a higher overall dynamical efficiency and more spin-up of the winds. Secondly, such large storms may be more resistant to vertical wind shear. As a result, RI seems to be especially favored when Ξ is large.

It is quite remarkable that an inner core structural/dynamical parameter has been found to explain as much variance as MPI. To measure whether whether Ξ can add independent information beyond what is known from the storm environment, and therefore be useful in a statistical-dynamical prediction scheme like SHIPS, a multiple linear regression model was constructed based on persistence, deep layer vertical wind shear, and MPI. Adding Ξ to this multiple linear regression model did not add significant skill, although this analysis is quite preliminary.[4] From this result, it seems possible that the inner core storm structure somehow incorporates the information contained in the environment. If so, this suggests the intriguing possibility that MPI theory can be somehow extended to include aspects of the inner core structure.

[3] This finding was first noted by Weatherford and Gray (1988).

[4] Since intensity change is a highly non-linear process, it is not at all certain that a multiple linear regression technique is the best way to measure the predictive utility of Ξ.

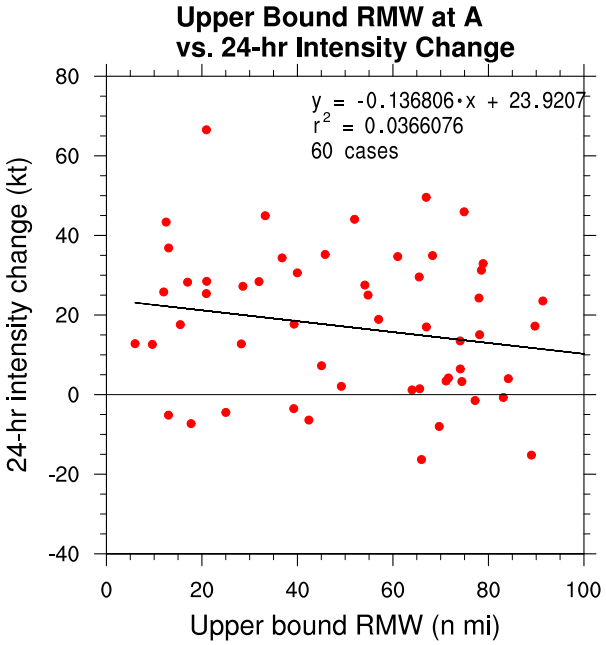

Figure 6: A scatter plot of upper bound r_{eye} vs. the subsequent 24-h intensity change after eye formation.

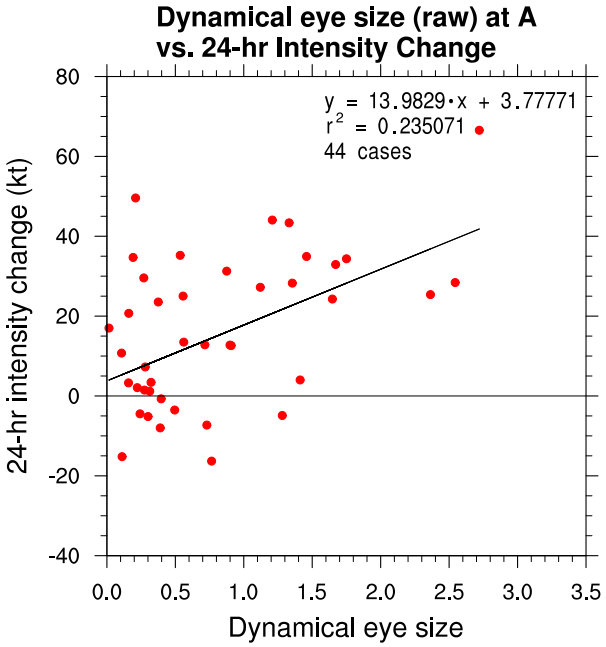

Figure 7: A scatter plot of the raw Ξ vs. the subsequent 24-h intensity change after eye formation.

ACKNOWLEDGMENTS

An enormous debt is owed to the brave flight crews of the 53rd Weather Reconnaissance Squadron and NOAA's Aircraft Operation Center who put themselves at risk each and every time they go out to collect these vital data. I also thank the following people for their assistance in obtaining the raw VDMs used in this study: Steve Feuer, Barry Damiano, John Pavone, Chris Sisko, Christopher Juckins, Mark Zimmer, Christopher Landsea, and Neal Dorst. My many questions about the VDM contents, format, history, and usage have been patiently answered by the previous people, and also by Eric Blake, Jonathan Talbot, Jack Parrish, and Nicholas Carrasco. Mary Haley provided very helpful advice on some of the programming aspects of this project. Mark DeMaria provided helpful feedback. The initial compilation of the VDM data set was supported by NASA/TCSP Grant NNG06GA54G and NSF Grants ATM-0332197 and ATM-0837932. The first author received support from the NCAR Advanced Study Program.

5. REFERENCES

References

Bister, M. and K. A. Emanuel, 1998: Dissipative heating and hurricane intensity. *Meteorol. Atmos. Phys.*, **65**, 233–240.

Jorgensen, D. P., 1984: Mesoscale and convective-scale characteristics of mature hurricanes. Part II: Inner core structure of Hurricane Allen (1980). *J. Atmos. Sci.*, **41**, 1287–1311.

Pendergrass, A. G. and H. E. Willoughby, 2009: Diabatically induced secondary flows in tropical cyclones. Part I: Quasi-steady forcing. *Mon. Wea. Rev.*, **137**, 805–821, doi:10.1175/2008MWR2657.1.

Schubert, W. H. and J. J. Hack, 1982: Inertial stability and tropical cyclone development. *J. Atmos. Sci.*, **39**, 1687–1697.

Shapiro, L. J. and H. E. Willoughby, 1982: The response of balanced hurricanes to local sources of heat and momentum. *J. Atmos. Sci.*, **39**, 378–394.

van Delden, A., 1989: On the deepening and filling of balanced cyclones by diabatic heating. *Meteorol. Atmos. Phys.*, **41**, 127–145.

Vigh, J. L., J. A. Knaff, and W. H. Schubert, 2012: A climatology of hurricane eye formation. *Mon. Wea. Rev.*, **140**, 1405–1426, doi:10.1175/MWR-D-11-00108.1.

Vigh, J. L. and W. H. Schubert, 2009: Rapid development of the tropical cyclone warm core. *J. Atmos. Sci.*, **66**, 3335–3350, doi:10.1175/2009JAS3092.1.

Weatherford, C. L. and W. M. Gray, 1988: Typhoon structure as revealed by aircraft reconnaissance. Part II: Structural variability. *Mon. Wea. Rev.*, **116**, 1044–1056.

Willoughby, H. E., F. D. Marks Jr., and R. J. Feinberg, 1984: Stationary and moving convective bands in hurricanes. *J. Atmos. Sci.*, **41**, 3189–3211.

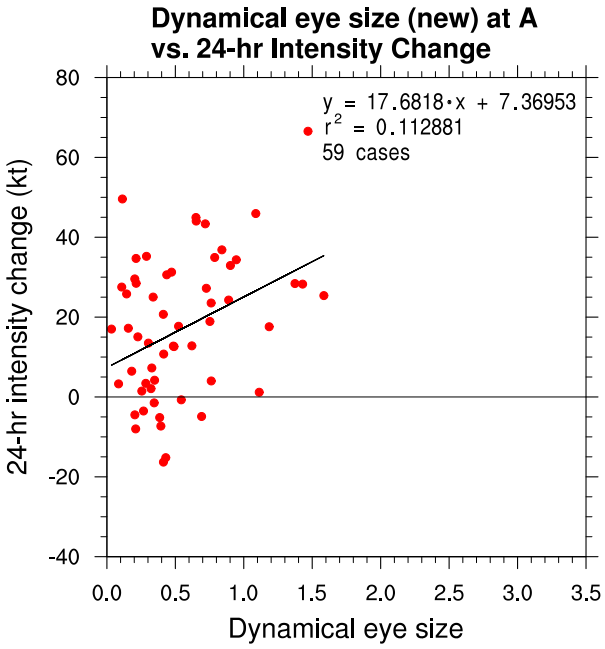

Figure 8: A scatter plot of the time-trended upper bound Ξ vs. the subsequent 24-h intensity change after eye formation.

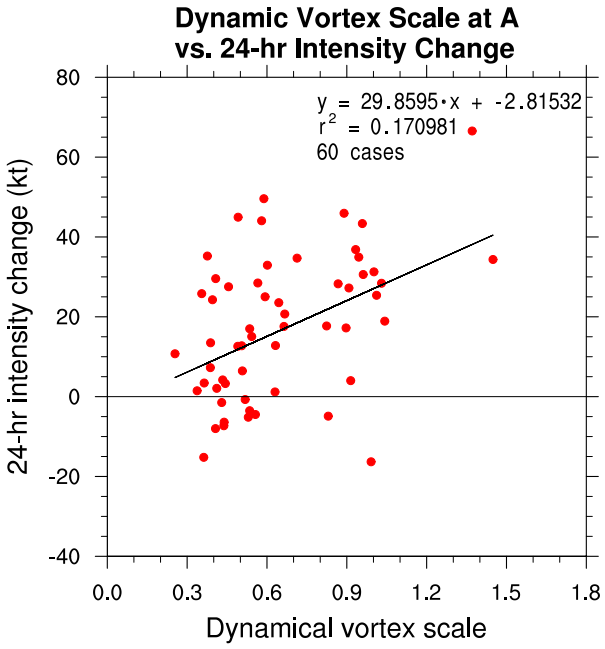

Figure 9: A scatter plot of the Dynamical Vortex Scale vs. the subsequent 24-h intensity change after eye formation.

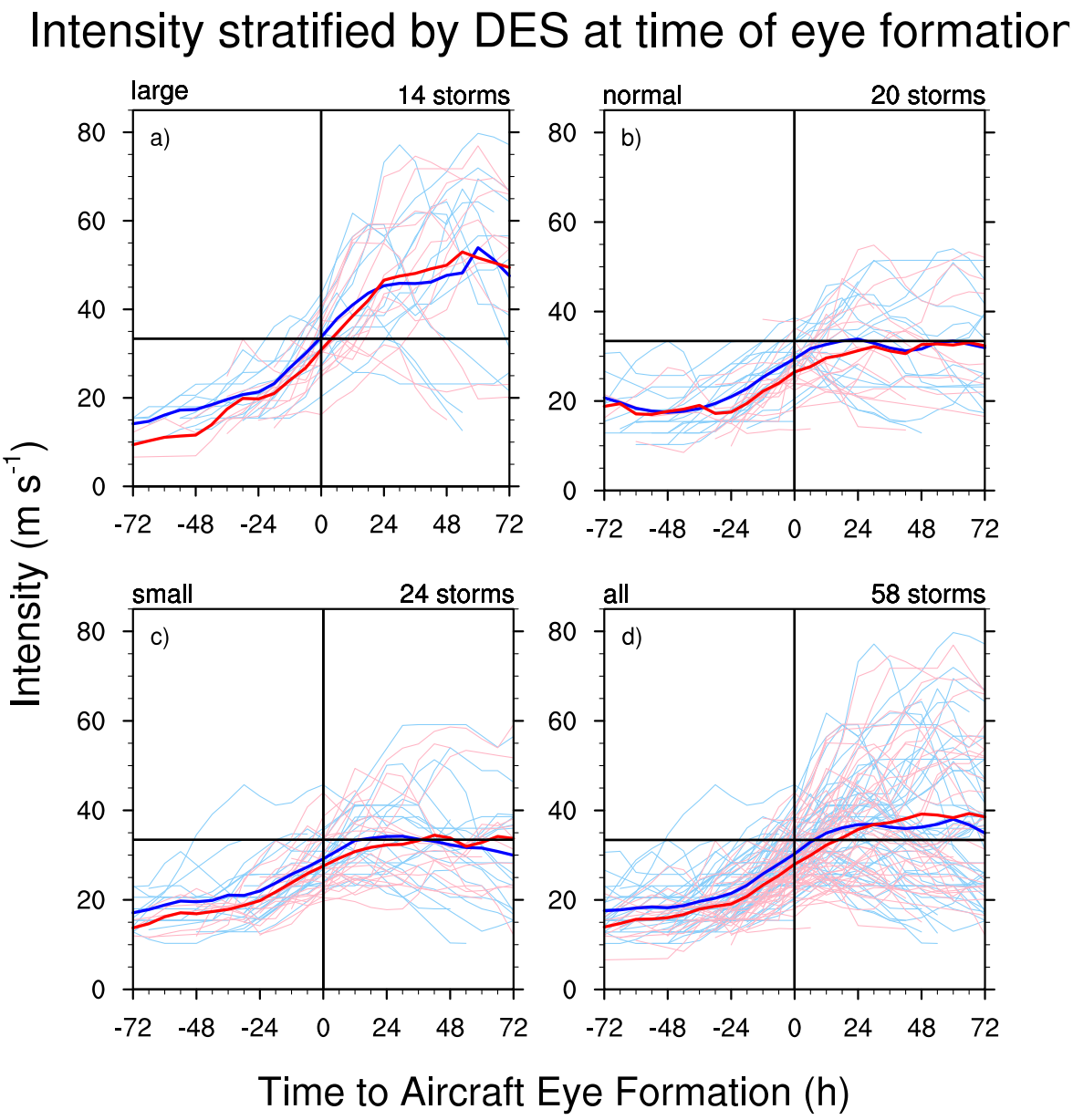

Figure 10: BT $v_{\max}$ and rFL $v_{\max}$ interpolated to various times before and after the first report of an open or closed aircraft eye. Each panel shows the individual intensity curves of storms and the composite mean intensity of those cases for (a) Ξ greater than 1.2, (b) Ξ between 0.4 and 1.2, (c) Ξ less than 0.4, and (d) all cases. Individual intensities of storms for that particular baseline are shown for both the BT $v_{\max}$ (thin light blue lines) and the rFL $v_{\max}$ (thin light pink lines). The mean intensities computed from the individual storms are also shown for both the BT $v_{\max}$ (thick blue line) and the rFL $v_{\max}$ (thick red line). For the reader's convenience, a vertical reference line has been added at zero on the time coordinate to indicate the time when aircraft first reported an eye. Similarly, a horizontal baseline has been added at $v_{\max} = 60$ kt.